ISBN: 978-3-95450-248-6 ISSN: 2673-5490 doi: 10.18429/JACoW-IPAC25-TUPB103

STATUS UPDATE OF THE LASER-HYBRID ACCELERATOR FOR RADIOBIOLOGICAL APPLICATIONS (LHARA)

W. Shields*, M. Pereira, John Adams Institute at Royal Holloway, University of London, UK
T.J. Kuo, K. Long, J. Pasternak, R. Razak, Imperial College, London, UK
C. Whyte, University of Strathclyde, Glasgow, UK
C. Hill, H. L. Owen, Cockcroft Institute, STFC Daresbury Laboratory, Warrington, UK

Abstract

The Laser-hybrid Accelerator for Radiobiological Applications (LhARA) represents a transformative approach to ion-beam therapy and radiobiological research. LhARA proposes to utilize a laser-driven proton and ion source, combined with advanced beam delivery systems, to provide highly flexible, high-repetition-rate, and ultra-short ion bunches suitable for radiobiological research. The LhARA project has entered a new phase of research and development following on from its first stage of preliminary activity. Here, we present a status update on recent LhARA progress. Highlights include an improved parametrised source description, the latest design of the FFA magnets including simulated fields and tune calculations in particle tracking, and updates to beam delivery schemes in LhARA's end stations for generating flexible beam conditions.

INTRODUCTION

LhARA is a proposed state-of-the-art particle accelerator that will serve a cutting edge radiobiological research program [1, 2]. LhARA will employ the transverse normal sheath acceleration (TNSA) mechanism in a laser-target acceleration scheme to generate proton bunches. A multi-stage facility, shown in Fig. 1, LhARA will transport short bunches of 10^9 protons at a nominal energy of 15 MeV $\pm 2\%$ at a 10 Hz repetition rate, a limit of the laser. These highly divergent beams will be captured with Gabor plasma lenses, yielding bunches between 1-3 cm in diameter. A matching arc will transport the beams vertically upwards after which a beam delivery system will provide further flexibility prior to delivery to a radiobiology end station.

LhARA's second stage will see the beam accelerated via a fixed field alternating gradient accelerator (FFA) which offers both variable energy and fast extraction, both requirements of the radiobiology community. LhARA's FFA will accelerate protons up to 127 MeV after which beams can be delivered to one of two high energy end stations. LhARA's FFA is a scaling spiral, 10 cell ring. Each cell contains a single combined-function spiral magnet. Previous iterations of the FFA design were unable to achieve sufficient vertical focusing to maintain orbit due to the fringe field in the 3D field map being longer than assumed during the original design. To correct this, the magnet spiral angle was changed to 53.9° and the machine re-tuned.

* william.shields@rhul.ac.uk

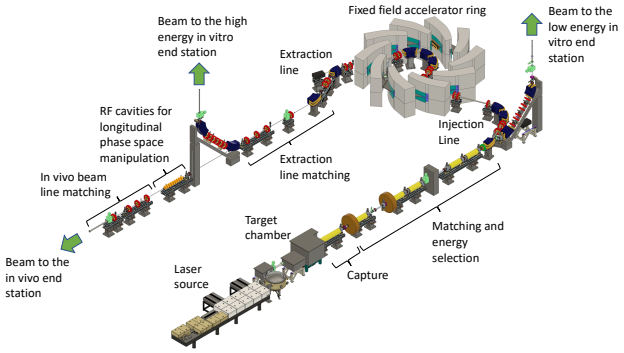

Figure 1: Schematic layout of the LhARA accelerator.

PARAMETERISED SOURCE DESCRIPTION

LhARA's previous source description in accelerator tracking simulations were shown to contain unphysical artefacts that are considered unreliable. Now, a parametrised beam description is used from which Monte Carlo particle energies are generated via inverse transform sampling. The kinetic energy spectrum of the TNSA model in [3] is given by

$$\frac{dN}{dK} = \frac{n_{e0} c_s t_{laser} S_{sheath}}{\sqrt{2KT_e}} \exp\left(-\sqrt{\frac{2K}{T_e}}\right), \quad (1)$$

where N is the number of protons produced per unit solid angle, K is the kinetic energy, n_{e0} and T_e are the hot electron density and temperature respectively, c_s is the proton acoustic velocity, t_{laser} is the laser pulse duration, and S_{sheath} is the effective area over which the TNSA mechanism takes place. This equation is unable to predict the high-energy cut-off known to occur in the TNSA process. To compensate, we apply the model described in [4], with the cut-off energy being given by

$$K_{max} = X^2 2Zm_e c^2 \sqrt{\frac{fP_{laser}}{P_R}}, \quad (2)$$

where Z is the charge, m_e is the electron mass, c is the speed of light, f is a energy conversion efficiency value, P_{laser} is the laser power, P_R is the relativistic power unit, and X is obtained by solving

$$\frac{t_{laser}}{t_0} = X\left(1 + \frac{1}{2}\frac{1}{1-X^2}\right) + \frac{1}{4}\ln\left(\frac{1+X}{1-X}\right), \quad (3)$$

ISBN: 978-3-95450-248-6 ISSN: 2673-5490 doi: 10.18429/JACoW-IPAC25-TUPB103

where t_0 is the time over which the acceleration may be treated as ballistic. A user defined low energy cut-off is applied to prevent the introduction of infinities in the inverse transform sampling as K approaches 0. This region of the spectrum is also less well understood experimentally and not of biological interest. The resulting Monte Carlo spectrum and theoretical spectrum from Eq. 1 are shown in Fig. 2.

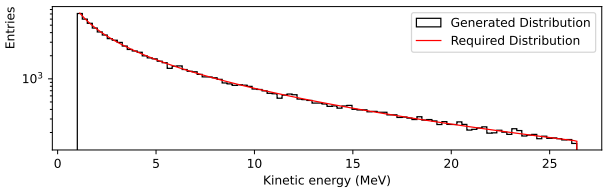

Figure 2: Monte Carlo generated kinetic energy spectrum (black) compared to the theoretical spectrum (red) with high energy and user-defined low energy cut-offs.

FFA MAGNETS

The goal of the FFA magnet design is zero chromaticity; this avoids resonance crossing in the tune space to avoid beam loss. One of the ways to achieve this is to arrange the magnetic field on the midplane with the scaling law. This has the advantage of optimizing for a single energy level naturally extends across the entire acceleration range. The integrated scaling law is defined as

$$BL(r) = BL_0 \left(\frac{r}{r_0} \right)^{k+1} \tag{4}$$

where r_0 is the reference radius chosen and BL_0 the integrated magnetic field at that radius. The integrated B field BL is defined as

$$BL(r) = \int B(r, \theta) r d\theta \tag{5}$$

where r and θ are cylindrical coordinates, and the field index k defined as:

$$k(r) = \frac{r}{BL} \frac{\partial BL}{\partial r} - 1 \tag{6}$$

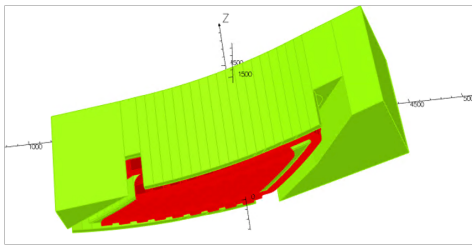

Figure 3: Opera 3D model showing the upper half of the magnet with trim coils wrapped around the pole. Clamps on either sides to contain the field.

The field profile is generated by a distribution of trim coils that cross the pole face and return on the side. The current settings are then adjusted for variable energy operation. The magnet, shown in Fig. 3 was designed in Opera 3D, with two different energy ranges investigated. The maximum energy case: 15 MeV at energy accelerated to 127 MeV and a lower energy case: 7 MeV at injection accelerated to 57 MeV. After the current settings were optimised, 3D field maps were obtained and tracked in Fixfield [5]. The results are shown in Fig. 4, with the working tune points avoiding any resonance up to the fourth order. A more detailed description of LhARA's FFA magnet design can be found in [6].

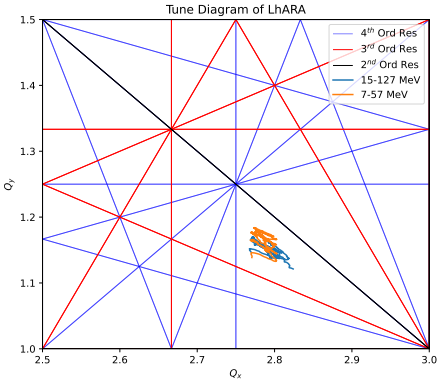

Figure 4: Ring tune variation of two energy ranges. The working tune points overlap and avoids any resonance up to the fourth order.

INJECTION LINE

The change in FFA spiral angle required the injection line to be redesigned to prevent the ring straight section crossing colliding with the FFA magnet, and to permit sufficient space for installation and maintenance of injection magnets.

The nominal injection line assumes initial conditions of $\beta_{x,y} = 25$ m, $\alpha_{x,y} = 0$, and $D_x = 0$ from stage 1. Optimising the stage 1 beam line to match these conditions proved challenging due to emittance growth during transit through the Gabor lenses, up to approximately 4.3×10^{-6} m rad at the injection line switching dipole. Stage 1 has therefore been optimised to meet a smaller $\beta_{x,y}$ of ~ 18 m. With this reduced β, the injection line quadrupoles are re-optimised in MADX [7], with the resulting optics seen in Fig. 5 in close agreement to the nominal design performance. The injection line is therefore considered strongly flexible.

BEAM DELIVERY SCHEMES

Magnetic Mini-Beam Focusing

Following on from the magnetic beam focusing quadrupole doublet configuration, presented in [8], where a line-focus minibeam was simulated; the current configuration is being developed to produce a spot-focus minibeam

ISBN: 978-3-95450-248-6 ISSN: 2673-5490 doi: 10.18429/JACoW-IPAC25-TUPB103

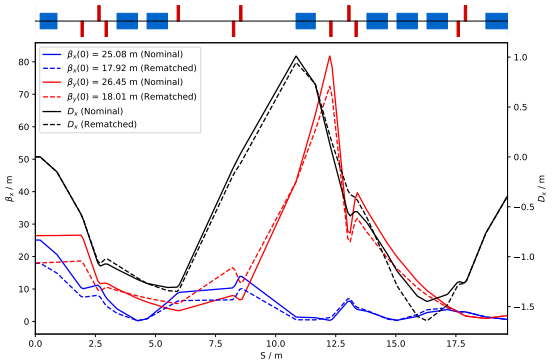

Figure 5: Horizontal (blue) and vertical (red) Twiss β functions and horizontal dispersion (black) in the FFA injection line. Both the nominal design (solid line) and rematched optics (dashed line) with modified initial conditions are shown.

from a 1 cm beam. This new configuration comprises of two quadrupole triplets, shown in Fig. 6. All optimisations have been carried out using the same method as [8].

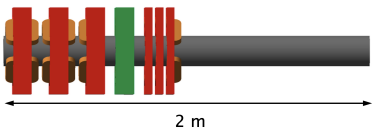

Figure 6: Magnetic beam focusing system with quadrupoles (red) and an octupole (green); after the end of the vertical arc leading to the Stage 1 in vitro end station.

Both quadrupole triplets consist of a defocusing magnet, a focusing magnet, and a second defocusing magnet. The first triplet has magnet lengths of 0.1 m with K_1 strengths of 30.26 m^{-2} and -53.39 m^{-2}, respectively. The second triplet has magnet lengths of 0.04 m and K_1 strengths of 302.56 m^{-2} and -551.73 m^{-2}. Due to their high magnetic fields and close proximity, they have been designed as permanent magnets to mitigate the high power consumption and currents required.

Figure 7 presents the beam size ($\sigma_{x,y}$) from the end of the vertical matching arc up to the Stage 1 in vitro end station, where $\sigma_{x,y}$ describes the rms beam radii. This focusing system gives a $\sigma_x \approx 0.74$ mm and $\sigma_y \approx 0.46$ mm, at the end of the system. This configuration only satisfies the condition to be classed as a minibeam ($\sigma \leq 0.5$ mm) in the y-z plane, so more optimisations will be necessary to reduce σ_x.

Beam Uniformity

Conventional beams at the end stations must achieve at least 95% transverse profile uniformity with minimal impact on delivered dose. Octupole-based magnetic shaping is a promising approach, although it produces a uniform region narrower than the full beam width [9]. The remaining non-uniform region would require collimation, reducing the effective dose. Octupoles are most effective under strong transverse asymmetry, and the uniform width is maximized

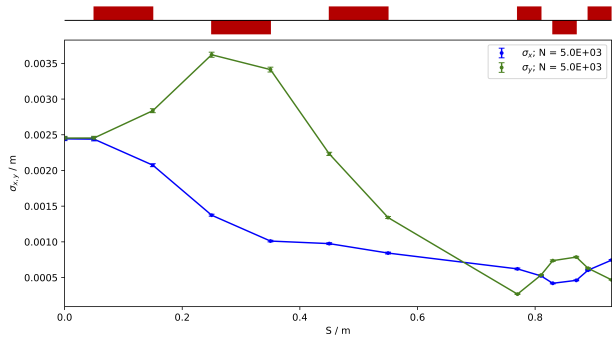

Figure 7: Horizontal (blue) and vertical (green) beam radii along the magnetic focusing system. The survey above the plot shows the positions of all the quadrupoles magnets (red).

when the phase advance to the target is approximately $n\frac{\pi}{2}$ [9]. The quadrupoles used for mini-beam focusing can be tuned to achieve the necessary asymmetry and phase advance.

An initial simulation in BDSIM [10], with an octupole acting in the x-plane and positioned as shown in Fig. 6, used a strength of $K_3 = -3905\,m^{-4}$ and produced the transverse phase space at the end station shown in Figure 8. This distribution achieves the target (95 ± 0.5) % uniformity in the x-plane within the predicted 1.88 cm width, capturing 55.7% of the beam.

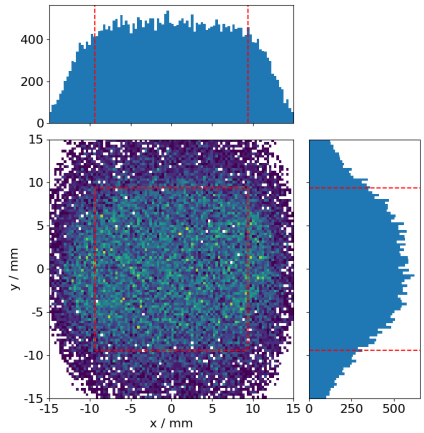

Figure 8: Transverse beam profile at the end of LhARA Stage 1 with an octupole acting on the x-axis. Red dashed lines indicate the predicted uniform region width of 1.88 cm.

SUMMARY & OUTLOOK

The most recent updates to the LhARA accelerator design have been presented. The Stage 1 design remains strong with the presented efforts demonstrating LhARA's flexibility. Stage 2 remains the primary focus going forwards, with the FFA magnet highlighting the excellent promise of the design.

ACKNOWLEDGEMENTS

This work is supported by the UKRI Infrastructure Fund ITRF project.

ISBN: 978-3-95450-248-6 ISSN: 2673-5490 doi: 10.18429/JACoW-IPAC25-TUPB103

REFERENCES

[1] G. Aymar *et al.*, "Laser-hybrid Accelerator for Radiobiological Applications (LhARA)", Imperial College London, UK, Conceptual Design Rep., CCAP-TN-01, July 2020. https://ccap.hep.ph.ic.ac.uk/trac/raw-attachment/wiki/Communication/Notes/CCAP-TN-01.pdf

[2] G. Aymar *et al.*, "LhARA: The Laser-hybrid Accelerator for Radiobiological Applications", *Front. Phys.*, vol. 8, Sept. 2020. doi:10.3389/fphy.2020.567738

[3] J. Fuchs *et al.*, "Laser-driven proton scaling laws and new paths towards energy increase", *Nat. Phys.*, vol. 2, pp. 48-–54, Dec. 2005. doi:10.1038/nphys199

[4] J. Schreiber *et al.*, "Analytical Model for Ion Acceleration by High-Intensity Laser Pulses", *Phys. Rev. Lett.*, vol. 97, p. 045005, July 2006. doi:10.1103/PhysRevLett.97.045005

[5] J.-B. Lagrange, "The Particle Tracking Code Fixfield", in *Proc. IPAC'21*, Campinas, Brazil, May 2021, pp. 1905–1906. doi:10.18429/JACoW-IPAC2021-TUPAB209

[6] T.-J. Kuo, J. Pasternak, and J.-B. Lagrange, "Design of FFA magnet for the laser-hybrid accelerator for radiobiological applications (LhARA)", presented at the 16th Int. Part. Accel. Conf. (IPAC'25), Taipei, Taiwan, Jun. 2025, paper WEPB087, this conference.

[7] L. Deniau *et al.*, "The Mad-X Program (Methodical Accelerator Design): User's Reference Manual", CERN, Geneva, Switzerland, May 2023. https://madx.web.cern.ch/madx/releases/last-rel/madxuguide.pdf

[8] R. Razak, "Development of novel magnetically-focussed minibeams for in vivo and in vitro end stations for LhARA", in *Proc. IPAC'24*, Nashville, TN, USA, May 2024, pp. 2649–2651. doi:10.18429/JACoW-IPAC2024-WEPR63

[9] Y. Yuri *et al.*, "Transformation of the Beam Intensity Distribution and Formation of a Uniform Ion Beam by Means of Nonlinear Focusing", *Plasma and Fusion Research*, vol. 9, p. 4406106, June 2014. doi:doi.org/10.1585/pfr.9.4406106

[10] L. J. Nevay *et al.*, "BDSIM: An accelerator tracking code with particle-matter interactions", *Comput. Phys. Commun.*, vol. 252, p. 107200, July 2020. doi:10.1016/j.cpc.2020.107200